Eur. Phys. J. Plus (2025) 140:819
https://doi.org/10.1140/epjp/s13360-025-06715-0

THE EUROPEAN PHYSICAL JOURNAL PLUS

Regular Article

Fast and thermal neutron measurements inside a fusion-oriented shielding mock-up

Fusion neutron shielding

A. Calamida[1,a], L. Russo[2], M. A. Caballero Pacheco[2], A. I. Castro Campoy[2], D. Dashdondog[2,3], R. Bedogni[2], D. Flammini[1], S. Cesaroni[1], A. Colangeli[1], F. Moro[1], G. Pagano[1], S. Loreti[1], A. Pietropaolo[1,2]

[1] ENEA - Nuclear Department, Frascati, Italy
[2] Istituto Nazionale Di Fisica Nucleare - Frascati National Laboratories, Frascati, Italy
[3] Università Di Torino, Turin, Italy

Received: 27 March 2025 / Accepted: 3 August 2025 / Published online: 2 September 2025

Abstract A Neutronics benchmark experiment was carried out at the Frascati Neutron Generator (FNG) operating at the ENEA Frascati research centre. The experiment aimed at using real-time neutron sensors to measure the spatial distribution of thermal and fast neutrons in a prototype shielding assembly exposed to 14 MeV fusion neutrons. The fast neutrons were measured exploiting the inelastic $^{12}C(n,\alpha)^{9}Be$ ($Q = -5.7$ MeV) and $^{28}Si(n,\alpha)^{25}Mg$ ($Q = -2.66$ MeV) reactions in a bare Silicon Carbide (SiC) solid state detector. The thermal neutrons were measured using an identical SiC detector covered by a ^{6}LiF neutron absorbing layer. The experimental results are eventually compared with dedicated FLUKA-INFN simulations.

1 Introduction

Tungsten mixed with an efficient neutron moderator (such as water or polyethylene) might represent an optimal shielding material for fusion experiments like DEMO, especially in regions where space constraints make difficult reaching the required neutron/gamma attenuation [1]. Evaluating the shielding performance of layered assemblies of tungsten and hydrogenated materials is a key activity for DEMO. In fact, tungsten is used in the first wall and in the divertor and the mock-up replicates the composition of the limiter. This material proved to have good shielding properties [1] with low neutron activation [2]. Also, the high melting temperature and high heat refractoriness, make tungsten the best choice as first wall component.

Neutron activation of thin foils of different materials is the classical method to characterize the neutron field inside a mock-up shielding assembly, as done for ITER [3] and DEMO [4, 5] experiments. This method is widely accepted, reliable and based on well-known activation cross sections. However, since the activation foils must be counted one by one, this method is time-consuming and requires considerable manpower. These measurements would be greatly simplified if an active neutron sensor was available to scan the volume of the mock-up shielding assembly like in [6].

The experiment presented in this work relies on two Silicon Carbon (SiC) solid state detector simultaneously acquired:

- A fast neutron sensor relying on a bare Silicon Carbide, hereafter named "bare-SiC";
- A thermal neutron sensor relying on a Silicon Carbide covered by a 30 μm thick ^{6}LiF layer, hereafter named "SiC + LiF".

The SiC diodes have been chosen because of their high radiation hardness [7–9].

Based on the previous simulations with MCNP5 Monte Carlo code [10] and the JEFF-3.3 nuclear data library [11], a prototype shielding assembly, made of layered tungsten, stainless steel foils and Perspex sheets, was built at the ENEA's Frascati Research Centre. An irradiation experiment with 14.1 MeV neutrons from the Frascati Neutron Generator (FNG) [12] was performed using different activation foils to map the neutron field along the axis of the assembly [13]. This work aims at:

- Validating the use of rad-hard Silicon Carbide sensors for mapping the thermal and fast neutron field within the assembly;
- Benchmarking a new FLUKA-INFN [14–16] model of the assembly.

2 The shielding assembly

According to the results of the pre-analysis [13], an experimental assembly made of densimet-180 (95% W, 3.4% Ni, 1.6% Fe), SS-316L and Perspex, the latter used to mimic water. The whole mock-up was assembled as shown in Fig. 1

[a] e-mail: alessandro.calamida@enea.it (corresponding author)

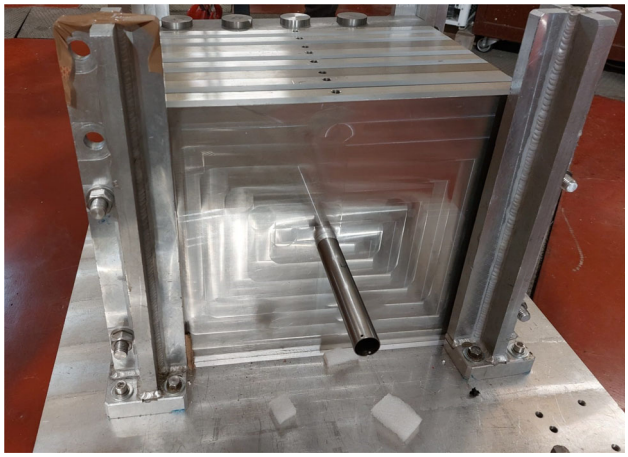

Fig. 1 Picture of the mock-up tested at FNG facility

Fig. 2 Inserts placed inside the hollow pipe to repeat the layered structure when the detectors are exposed. These have thickness 3 cm (densimet-180), 2.2 cm (SS-316L) and 2 cm (perspex)

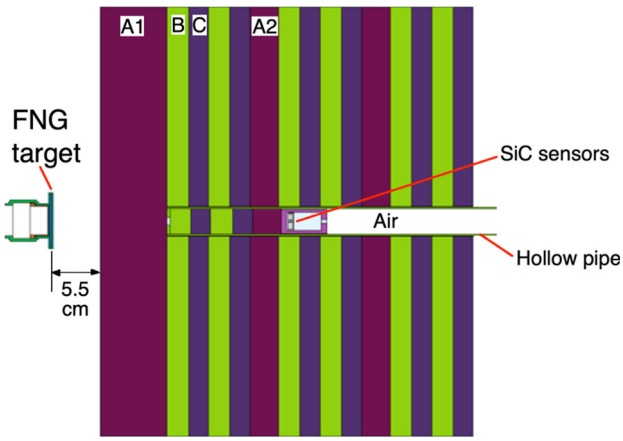

Fig. 3 Representation of mock-up layers in the simulation model. $A1$ = densimet-180 (7 cm thick); B = SS-316L (2.2 cm thick); C = perspex; $A2$ = densimet-180 (3 cm thick)

1. The sensor can be introduced into the assembly through a central cylindrical well and a cylindrical hollow pipe. A set of cylindrical inserts of densimet-180, stainless steel and perspex allows to reproduce inside the pipe the radial layout of the mock-up, see Fig. 2. These have the following thickness:

- densimet-180: ~ 3.00 cm;
- stainless steel 316L: ~ 2.21 cm;
- perspex: ~ 2.03 cm.

Both SiC detectors were placed in various positions inside the cylindrical well.

The dimensions of the mock-up are $48 \times 42 \times 39.4$ cm^3. A 2D representation of the layered structure of the mock-up is shown in Fig. 3. The air space behind the detectors is needed to accommodate the electrical cables. The layers composing the mock-up have the following thickness:

- One slab of densimet-180 of thickness 7 cm (A1), featuring no central hole;
- Two slabs of densimet-180 of thickness 3 cm (A2) each;
- Six slabs of stainless steel 316L of thickness 2.4 cm (B) each;
- Six slabs of perspex of thickness 2 cm (C) each.

The front face of the mock-up was placed at a distance of 5.5 ± 0.2 cm from the FNG neutron emitting target, see Fig. 4. The positions of the detectors during the exposure are listed in Table (1) together with the amount of shielding interposed between the

Fig. 4 Experimental setup of the measurements at FNG with the shielding mock-up

assembly front face and the detectors. The measurements took place at FNG in D-T mode at an emission rate of about $0.5 \div 1.0 \times 10^{10}$ n/s^{-1}. The average neutron energy impacting on the front face of the mock-up was of 14.1 MeV.

3 The experimental technique

The detectors are commercially available, windowless, Silicon Carbide Schottky diodes with active an area of 7.6 mm^2. The sensitive thickness, corresponding to the depleted layer of the diode, is 1.8 mm with 12 V inverse biasing. The SiC+LiF and bare-SiC detectors were connected to a dual channel analogue electronic board. Every channel is composed by a preamplifier CREMAT CR110 and a CREMAT CR200 shaper amplifier featuring 1 μs shaping time. The output signal was digitized and elaborated in terms of pulse height distribution (PHD), see Fig. 7.

The fast neutron component was measured using the bare-SiC exploiting the following inelastic reactions of the 14.7 MeV neutrons:

- $^{12}C(n, \alpha)^{9}Be$ with threshold energy: $E_{th} = 5.7$ MeV;
- $^{28}Si(n, \alpha)^{25}\,Mg$ with threshold energy: $E_{th} = 2.1$ MeV.

The typical PHD of the energy released by the secondary α particles from these inelastic reactions is shown in Fig. 7 ("bare curve").

The thermal neutron component was measured using the SiC+LiF featuring a ~ 30 μm layer of ^{6}LiF exploiting the reaction:

$$^{6}Li + n- \rightarrow \alpha + T\,(Q \cong 4.7 \text{ MeV}) \tag{1}$$

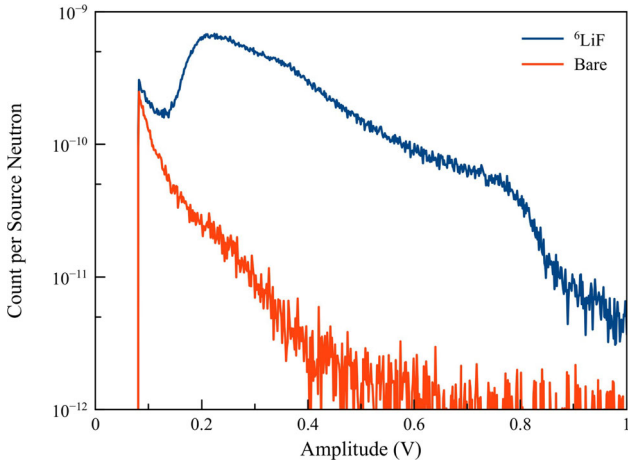

Fig. 5 Representative PHD recorded by the SiC + LiF (blue) and the bare-SiC (red) detectors

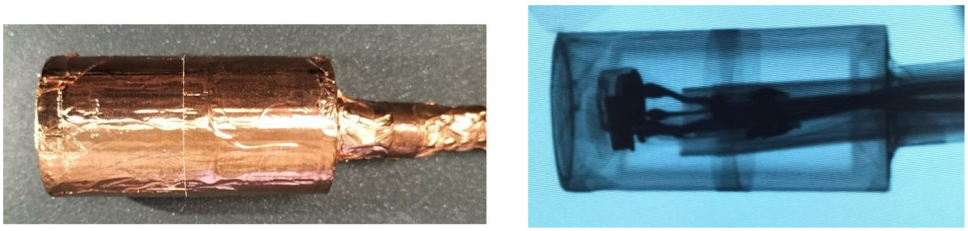

Fig. 6 (*Left*) Pictures of the detector assembly with the electromagnetic shield (*Right*) X-rays image of both detectors

The thickness of the ^{6}LiF converter layer was chosen to maximize the detection efficiency [17]. The $^6Li(n, \alpha)T$ reaction cross sections decrease rapidly with the energy, thus making the detector mostly sensitive to thermal neutrons. The very thin active thickness of the sensor (1.8 mm) prevents γ-rays to produce detectable signals. The α-particles and tritons resulting from the reaction (1) release all possible energies from zero (particles produced deep in the ^{6}LiF converter, degraded in the converter and barely reaching the sensor) up to a maximum of 2.05 MeV (total α-particles energy) or 2.73 MeV (total T energy). With reference to the PHDs of Fig. 5 (^{6}LiF curve), the broad peak at about 0.25 V (0.8 MeV in terms of released energy) represents the α-particles generated in proximity of the sensor and crossing its surface with nearly perpendicular incidence angle. The α-particles at larger angles release more energy with a maximum at 2 MeV, corresponding to particles generated in proximity of the sensor, crossing its surface with gazing angles and completely stopped. The endpoint at about 0.9 V (2.75 MeV in term of released energy) corresponds to the tritons generated in proximity of the sensor, crossing its surface with grazing angles and completely stopped.

The "thermal neutron" PHD is obtained by subtracting the PHD of the bare-SiC from the one of the SiC+LiF. In order to eliminate the non-neutron events in the PHD, a 130 mV threshold in terms of signal amplitude was set for both detectors. The total neutrons counts were obtained from the cumulative PHD above the threshold. These were in turn normalized to the total neutrons emitted in a specific run, obtaining the "normalized counts", C_n.

To simultaneously measure thermal and fast neutron fields, the bare-SiC and the SiC+LiF detectors were embedded in a cylindrical plastic box covered by a conductive electromagnetic shield. Figure 6 shows a picture and an X-rays image of the detector assembly.

The SiC+LiF was calibrated in terms of thermal neutron fluence using HOTNES facility [18–20]. The bare-SiC, instead, was calibrated in term of 14 MeV neutron fluence using the FNG direct beam, in air, without the mock-up at the distances of 10, 15 and 20 cm from the target. The two calibration coefficients are:

- For the SiC + LiF: $k_{SiC+LiF} = (1.847 \pm 0.018) \times 10^{-3}$ cm^2;
- For the bare-SiC: $k_{bare-SiC} = (2.23 \pm 0.11) \times 10^{-5}$ cm^2.

The repeatability of C_n, tested via repeated exposures in Pos 4 (see Tab. 1) for a total number of emitted neutrons of $\sim 3 \times 10^{12}$, resulted to be within $\pm 3.4\%$ (1 s.d.) for SiC+LiF and $\pm 4.5\%$ for bare-SiC.

The whole experimental setup was reproduced by means of the Monte Carlo (MC) code FLUKA-INFN, see Fig.

3. The whole FNG machine and bunker have been accurately reproduced and a dedicated source accurately modelled the FNG neutron production.

4 Results and discussion

The computational and experimental results for the thermal neutrons as a function of the detector position within the mock-up are given in Fig. 7, where:

Table 1 Position of the detectors during the exposure

Position	Shielding	Depth (cm)
Pos 1	A1	.0 ± 0 7.5
Pos 2	Pos 1 + B	.2 ± 0 9.5
Pos 3	Pos 2 + C	.3 ± 011.5
Pos 4	Pos 3 + B	.6 ± 013.5
Pos 5	Pos 4 + C	.7 ± 015.5
Pos 6	Pos 5 + A2	.7 ± 018.5
Pos 7	Pos 6 + B + C	.8 ± 022.5
Pos 8	Pos 7 + B + C	.10 ± 027.50
Pos 9	Pos 8 + A2	.10 ± 030.50
Pos 10	Pos 9 + B + C	.4 ± 034.5
Pos 11	Pos 10 + B + C	.5 ± 038.5

Materials are labelled as: $A1$ = densimet-180 (7 cm thick); B = SS-316L (2.2 cm thick); C = perspex; $A2$ = densimet-180 (3 cm thick). The listed shielding is interposed between the assembly front face and the detector

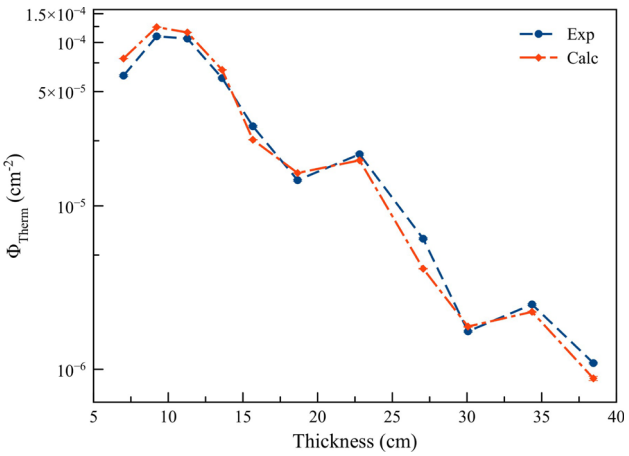

Fig. 7 Experimental and simulated thermal neutron fluence per emitted neutron inside the mock-up as a function of the detector position. For each data point, the uncertainty is smaller than the symbol. Dashed line is only a guide for the eye

- The experimental points, representing the measured thermal neutron fluence per source neutron, $\Phi_{T\,herm}$, were obtained by multiplying the quantity C_n (SiC + LiF) by the due calibration coefficient $k_{Sic+LiF}$ obtained in the reference thermal neutron facility HOTNES (see Sect. 3);
- The computational points, representing the simulated thermal neutron fluence per source neutron, were obtained with FLUKA-INFN by scoring the neutron fluence below 0.5 eV in a volume corresponding to the ^{6}LiF radiator of the sensor. The simulation was performed in a realistic scenario including the detector.

The behaviour of the experimental and calculated neutron fluence is similar.

It can be seen that $\Phi_{T\,herm}$ features a general decreasing trend, due to the combination of the neutron scattering in densimet and steel, followed by slowing-down and capture in the Perspex. Superimposed to this trend, local maxima occur after every densimet layer. These are likely ascribable to $(n, 2n)$ multiplication reactions in tungsten, featuring a threshold of 10 MeV and cross section of $\sigma \sim 1.8$ b at 14.1 MeV. Multiplied neutrons in the MeV region are in turn moderated by the surrounding materials, producing the observed local increases in the thermal neutron fluence.

In Fig. 8 the *C/E* ratio (i.e. the ratio between the calculated, C, and experimental, E, fluence) is plotted for the thermal neutrons fluence. This ratio oscillates in a range of $0.65 \div 1.27$ with a standard deviation of $\sigma \sim 18\%$. Uncertainty bars also include a contribution of about $\pm 15\%$, coming from the uncertainty in the detectors positions inside the mock-up. This contribution was evaluated by means of a series of simulations by moving the detectors up to ± 5 mm from their nominal position respect to the FNG's target.

In Fig. 9, the results for the fast neutron fluence are shown. Both experimental and calculated fluence decrease exponentially inside the mock-up, allowing a calculation of Tenth Value Layer ($TV\,L$) of about 12.5 cm for both plots. The simulated results are compatible in the limit of the error with the experimental ones. The *C/E* ratio for the fast neutrons is shown in Fig. 10. It oscillates between $0.897 \div 1.02$ with a standard deviation $\sigma \sim 5\%$. The simulations seem to better reproduce the experimental trend, featuring less oscillations as compared to the thermal neutron case. Uncertainty bars also include a contribution of about $\pm 5 \div 6\%$, coming from the uncertainty in the detectors position inside the mock-up. This contribution was evaluated by means of a series of dedicated simulations by moving the detectors up to $\pm 5\%$ from their nominal position respect to the FNG's target like in the thermal case.

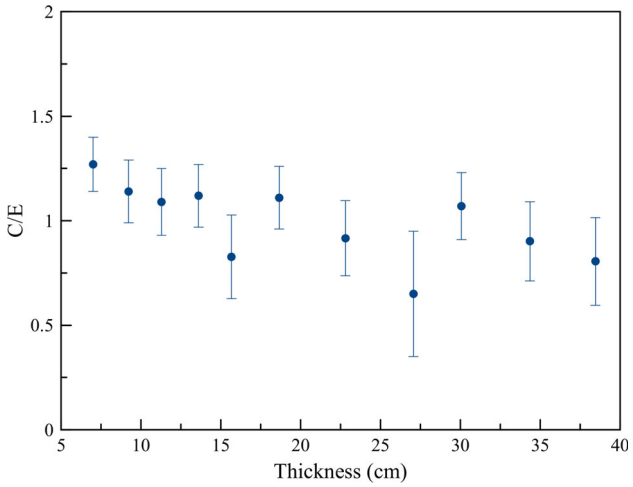

Fig. 8 *C/E* ratio for the thermal fluence. The errors consider also the uncertainty coming from the detector position error

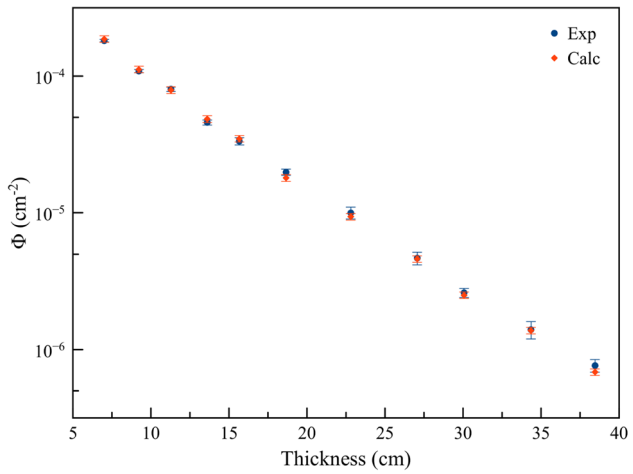

Fig. 9 Experimental and simulated fast neutron fluence per emitted neutron inside the mock-up as a function of the detector position

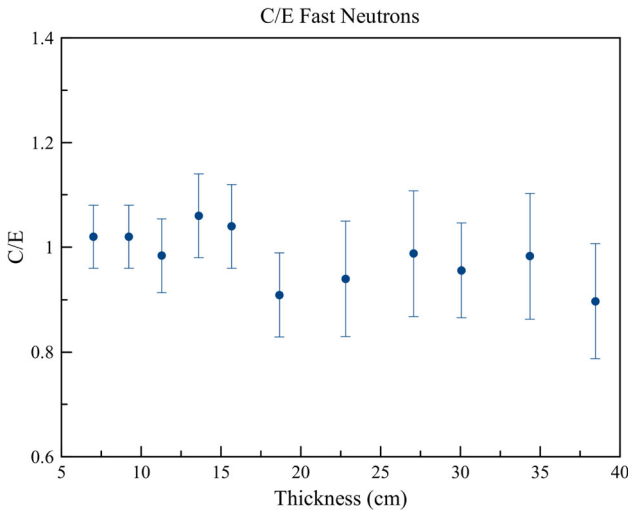

Fig. 10 *C/E* ratio for the fast fluence. The errors consider also the uncertainty coming from the detector position error

5 Conclusions

The thermal and the fast neutron field inside the mock-up were successfully measured using two SiC detectors. The results show the same behaviour for the active measurements and the activation foils ones. The results are also compatible with the simulations made with the FLUKA-INFN MC code.

The thermal and the fast neutron field inside the mock-up were successfully measured using active SiC detectors, exposed bare or coated with ^{6}LiF to detect fast or thermal neutrons, respectively. The measured variations of these field components within the layered Tungsten-perspex shielding mock-up are in agreement with the FLUKA predictions. Small deviations are likely due to uncertainties in the detectors positioning, as even a displacement of ± 0.5 cm may lead to a fluence variation as large as $\sim 15\%$ or more. Previous measurements with foil activation [13] provided similar trends. Radiation-hard Silicon carbide-based active neutron detectors proved to be a good method to map neutron fields in fusion-relevant experimental benchmarks.

Simulations with the MCNP MC code are also foreseen in the near future to study if the results will be compatible with the FLUKA ones. Moreover, this measurement approach will be tested for future experimental campaigns. A different type of mock-up made of various type of concrete will be studied and the neutron field inside it will be measured using the same detectors of this paper. Moreover, MC simulations will be made to verify the consistency of the experimental data using both the FLUKA and MCNP MC codes.

Acknowledgements I want to thank the CRESCO facility because the computing resources and the related technical support used for the simulations of this thesis have been provided by CRESCO/ENEAGRID High Performance Computing infrastructure and its staff [21]. CRESCO/ENEAGRID High Performance Computing infrastructure is funded by ENEA, the Italian National Agency for New Technologies, Energy and Sustainable Economic Development and by Italian and European research programmes, see Ref. [21] for information.

Funding Open access funding provided by Ente per le Nuove Tecnologie, l'Energia e l'Ambiente within the CRUI-CARE Agreement.

Data Availability Statement The data sets generated during and/or analysed during the current study are available from the corresponding author on reasonable request. The manuscript has associated data in a data repository.

References

1. S. Akbas et al., Neutron shielding calculation for DEMO-Prad/SXR measurement system. Phys. Plasmas **31**, 033112 (2024)
2. S. Noce et al., Neutronics analysis and activation calculation for Tungsten used in the DEMO divertor targets: a comparative study between the effects of WCLL and HCPB blanket, different W compositions and Chromium. Fusion Eng. Des. (2021). https://doi.org/10.1016/j.fusengdes.2021.112428
3. P. Batistoni *et al.*, Validation of FENDL-2.1 nuclear data library for use in ITER nuclear analysis.
4. P. Batistoni et al., Neutronics benchmark experiment on tungsten. J. Nucl. Mater. **329–333**, 683–686 (2004)
5. https://nbn-resolving.org/urn:nbn:de:swb:14-1096547324156-18744.
6. S. Unholzer et al., Measurement and analysis of neutron and photon flux spectra in an ITER shield mockup with open channel and cavity. Journ. of Nucl. Phys. **1**, 243–247 (2000)
7. M. Costa et al., Intense thermal neutron fields from a medical-type LINAC: the E LIBANS project. Rad. Prot. Dos. **180**, 273–277 (2018)
8. M. Treccani et al., Developing radiation resistant thermal neutron detectors for the E LIBANS project: preliminary results. Radiat. Prot. Dosim. **180**, 304–308 (2018)
9. R. Bedogni et al., On neutron detection with silicon carbide and its resistance to large accumulated fluence. Eur. Phys. J. Plus **137**, 1358 (2022)
10. *MCNP-A General Monte Carlo cod for Neutron and Photon Transport*, J. Bries Meister Ed. Los Alamos National Laboratory Report La-7396-M, Rev. 2, Sept. (1986).
11. J. Rowlands *et. al.*, *The JEF-2.2 nuclear data library*, JEFF Report 17 (2000).
12. M. Martone et al., The 14 MeV frascati neutron generator (FNG). Journ. Nucl. Mat. **212**, 1661–1664 (1994)
13. D. Flammini *et. al.*, Tungsten benchmark shielding experiment at the Frascati Neutron Generator, submitted to FED (2025)
14. A. Ferrari *et al.*, *FLUKA: a multiparticle transport code*, CERN-2005–010, INFN TC 05/11, SLAC-R-773, 2005.
15. T.T. Bohlen et al., The FLUKA code: developments and challenges for high energy and medical applications. Nucl. Data Sheets **120**, 211–214 (2014)
16. F. Ballarini et al., The FLUKA code: overview and new developments. EPJ Nucl. Sci. Technol. **10**, 16 (2024)
17. R. Bedogni et al., Nuc. Inst. Meth. A **1018**, 165855 (2021)
18. R. Bedogni et al., Nucl. Instrum. Methods Phys. Res. A. **843**, 18–21 (2017)
19. R. Bedogni et al., Appl. Radiat. Isot. **843**, 68–72 (2017)
20. A. Sperduti et al., J. Instrum. **12**, P12029 (2018)
21. F. Ian-none *et. al.*, *CRESCO ENEA HPC clusters: a working example of a multifabric GPFS Spectrum Scale layout*, 2019 International Conference on High Performance Computing & Simulation (HPCS), Dublin, Ireland (2019), pp. 1051–1052, https://doi.org/10.1109/HPCS48598.2019.9188135.